Radiology

ORIGINAL RESEARCH • NEURORADIOLOGY

High-Resolution Motion-corrected 7.0-T MRI to Derive Morphologic Measures from the Human Cerebellum in Vivo

Nikos Priovoulos, PhD • Mads Andersen, PhD • Serge O. Dumoulin, PhD • Vincent O. Boer, PhD • Wietske van der Zwaag, PhD

From the Spinoza Centre for Neuroimaging, Royal Netherlands Academy of Arts and Sciences (KNAW), Meibergdreef 75, 1105 BK Amsterdam, the Netherlands (N.P., S.O.D., W.v.d.Z.); Computational Cognitive Neuroscience and Neuroimaging, Netherlands Institute for Neuroscience, Amsterdam, the Netherlands (N.P., S.O.D., W.v.d.Z.); Philips Healthcare, Copenhagen, Denmark (M.A.); Lund University Bioimaging Centre, Lund University, Lund, Sweden (M.A.); Department of Experimental and Applied Psychology, Vrije Universiteit Amsterdam, Amsterdam, the Netherlands (S.O.D.); Department of Experimental Psychology, Utrecht University, Utrecht, the Netherlands (S.O.D.); and Danish Research Centre for Magnetic Resonance, Centre for Functional and Diagnostic Imaging and Research, Copenhagen University Hospital Hvidovre, Hvidovre, Denmark (V.O.B.). Received April 23, 2022; revision requested June 21; revision received October 12; accepted November 15. **Address correspondence to** N.P. (email: *n.Priovoulos@spinozacentre.nl*).

W.v.d.Z. supported by a Nederlandse Organisatie voor Wetenschappelijk Onderzoek (NWO) VIDI grant (TTW VI.Vidi.198.016).

Conflicts of interest are listed at the end of this article.

See also the editorial by Dietrich in this issue.

Radiology 2023; 000:1–9 • https://doi.org/10.1148/radiol.220989 • Content codes: NR MR

Background: The human cerebellum has a large, highly folded cortical sheet. Its visualization is important for various disorders, including multiple sclerosis and spinocerebellar ataxias. The derivation of the cerebellar cortical surface in vivo is impeded by its high foliation.

Purpose: To image the cerebellar cortex, including its foliations and lamination, in less than 20 minutes, reconstruct the cerebellocortical surface, and extract cortical measures with use of motion-corrected, high-spatial-resolution 7.0-T MRI.

Materials and Methods: In this prospective study, conducted between February 2021 and July 2022, healthy participants underwent an examination with either a 0.19 × 0.19 × 0.5-mm^3, motion-corrected fast low-angle shot (FLASH) sequence (14.5 minutes) or a whole-cerebellum 0.4 × 0.4 × 0.4-mm^3, motion-corrected magnetization-prepared 2 rapid gradient-echo (MP2RAGE) sequence (18.5 minutes) at 7.0 T. Four participants underwent an additional FLASH sequence without motion correction. FLASH and MP2RAGE sequences were used to visualize the cerebellar cortical layers, derive cerebellar gray and white matter segmentations, and examine their fidelity. Quantitative measures were compared using repeated-measures analyses of variance or paired *t* tests.

Results: Nine participants (median age, 36 years [IQR, 25–42 years; range, 21–62 years]; five women) underwent examination with the FLASH sequence. Nine participants (median age, 37 years [IQR, 34–42 years; range, 25–62 years]; five men) underwent examination with the MP2RAGE sequence. A susceptibility difference between the expected location of the granular and molecular cerebellar layers was visually detected in the FLASH data in all participants. The segmentations derived from the whole-cerebellum MP2RAGE sequence showed the characteristic anatomic features of the cerebellum, like the transverse fissures and splitting folds. The cortical surface area (median, 949 cm^2 [IQR, 825–1021 cm^2]) was 1.8 times larger, and the cortical thickness (median, 0.88 mm [IQR, 0.81–0.93 mm]) was five times thinner than previous in vivo estimates and closer to ex vivo reference data.

Conclusion: In vivo imaging of the cerebellar cortical layers and surface and derivation of quantitative measures was feasible in a clinically acceptable acquisition time with use of motion-corrected 7.0-T MRI.

Supplemental material is available for this article.

The human cerebellum has approximately one-eighth the volume of the neocortex but a cortical sheet with a similar surface area (1). The cerebellar cortex is a prevalent lesion site for various disease processes, including multiple sclerosis (2,3), spinocerebellar ataxias (4), and alcoholism (5).

The cerebellar cortex has a regular circuit characterized by the granular cells (granular layer: 250–350 μm wide) that output to the Purkinje cells (Purkinje layer: 12 μm) through the parallel fibers (molecular layer: 250–350 μm). Beams of parallel fibers underlie the characteristic cerebellar mediolateral folds (500–1000 μm) (6). Despite its importance, this mesoscopic scale of the cerebellar architecture is underexamined in humans: Current in vivo techniques are limited to gross anatomic features, such as the main cortical branches, due to inadequate resolution (1). As a result, clinical measures successfully used in the cerebral cortex, such as cortical thickness, volume, and myeloarchitecture/function correlates, have not been applied with high fidelity in the cerebellum (1). This hinders examination of the cerebellum in disease.

Herein, we combined methodologic advances in image acquisition and analysis to image the cerebellar cortex, including its foliations and lamination, with use of in vivo 7.0-T MRI to improve the signal-to-noise ratio and signal-to-noise efficiency. We modified two MRI pulse sequences targeted at imaging the cortical surface and intracortical lamination, respectively, to translate this higher signal-to-noise ratio to spatial resolution

Abbreviations

FLASH = fast low-angle shot, FOV = field of view, GM = gray matter, MP2RAGE = magnetization-prepared 2 rapid gradient echo, WM = white matter

Summary

Motion-corrected MRI at 7.0 T can visualize the in vivo cerebellar surface and cortical layers, with a spatial resolution of 0.4 mm isotropic up to 0.19 mm nonisotropic.

Key Results

- In a prospective study of nine healthy participants, a susceptibility difference between the inner and outer cerebellar cortex visualized the granular and molecular cerebellar cortical layers in all participants.
- The motion-corrected magnetization-prepared 2 rapid gradient-echo, or MP2RAGE, sequence with an isotropic in-plane spatial resolution of 0.4 mm resolved the cerebellocortical fissures in all participants; the median cortical surface area was 1.8 times larger and the median cortical thickness 5 times thinner compared with T1-weighted sequences with a spatial resolution greater than 0.75 mm.
- The cerebellocortical fissures were successfully computationally unfolded in all participants, revealing the continuous cerebellar cortical sheet.

(up to 200 μm). When the voxel size becomes that small, the effective spatial resolution is limited by involuntary patient motion (7). We therefore interleaved our MRI sequences with rapidly sampled whole-head fat images (8), with which we prospectively corrected participant motion. We aimed to examine the utility of our high-resolution, motion-resistant method in noninvasive imaging of the cerebellar cortex in a clinically applicable time.

Materials and Methods

Participants

Following approval of this prospective study by the local ethical committee, included participants provided written informed consent. The participants were screened before the experiments to ensure MRI compatibility (Fig 1). Nine healthy participants were scanned in a 7.0-T MRI scanner (Achieva, Philips Healthcare) using a two-channel transmit and 32-channel receive whole-head coil (Nova Medical) with a sequence aimed at imaging layers within the cerebellar cortex. Additionally, nine healthy participants completed a sequence that visualized the whole cerebellar cortex (three overlapping participants between groups). The images were visually inspected (N.P., with 7 years of MRI acquisition experience) for image quality (eg, B_1 inhomogeneity artifacts) and rejected if necessary. The study was conducted between February 2021 and July 2022.

Cerebellar Cortical Layers

The cerebellar cortical depth sequence consisted of a high-resolution in-plane T2*-weighted three-dimensional fast low-angle shot (FLASH) sequence (field of view [FOV], 210 × 210 × 15 mm^3; repetition time msec/echo time msec, 37.12/20; flip angle, 13°; matrix, 1120 × 1120 × 30; voxel size, 0.19 × 0.19 × 0.5 mm^3; sensitivity encoding$_{y/z}$, 1.5/1; acquisition time, 8 minutes). This sequence covered only part of the cerebellar cortex, with the section orientation placed obliquely so that it was perpendicular to the cortex and parallel to the direction of least anatomic variance (Figs 2A, S1; Appendix S1). The echo time was set close to the gray matter (GM) T2* value (approximately 23 msec) to maximize magnitude and phase contrast within the cerebellar GM (9). This FLASH sequence was segmented (acquisition time of the shot, 2 seconds) and interleaved (10) with fat navigators (three-dimensional echo-planar imaging with a fat-selective binomial excitation pulse; FOV, 240 × 240 × 120 mm^3; matrix, 120 × 120 × 60; voxel size, 2 × 2 × 2 mm^3; 5.65/1.88; acquisition time of the volume, 550 msec; flip angle, 1°; sensitivity encoding$_{y/z}$, 4/2; acquisition time of the fat navigator volume, 0.55 second) (11). A prospective motion correction algorithm realigned the reconstructed fat navigators in real time, updated the FOV (wait time, 0.9 second) (8), and reacquired shots with large movement (>0.5 mm on a 64-mm-radius sphere; total acquisition time was approximately 14.5 minutes). For four participants, an additional scan was acquired without prospective motion correction to evaluate the motion correction efficacy (Fig 2B–2D).

Whole–Cerebellar Cortex Sequence

The whole–cerebellar cortex sequence consisted of a magnetization-prepared 2 rapid gradient-echo (MP2RAGE) sequence (FOV, 210 × 120 × 60 mm^3; 5.65/1.88; inversion time 1/inversion time 2, 1000/2900 msec; flip angle for inversion times 1

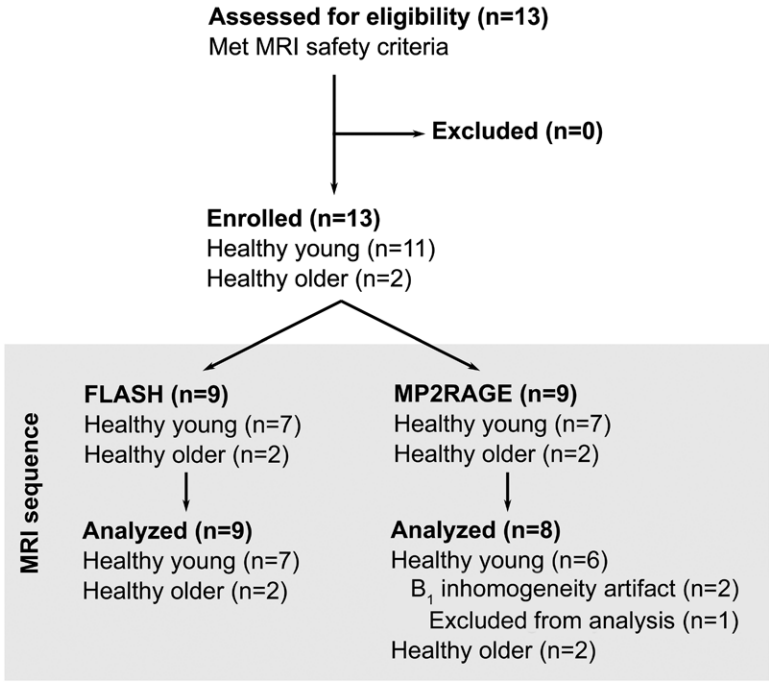

Figure 1: Flowchart of participant recruitment. FLASH = fast low-angle shot, MP2RAGE = magnetization-prepared 2 rapid gradient echo.

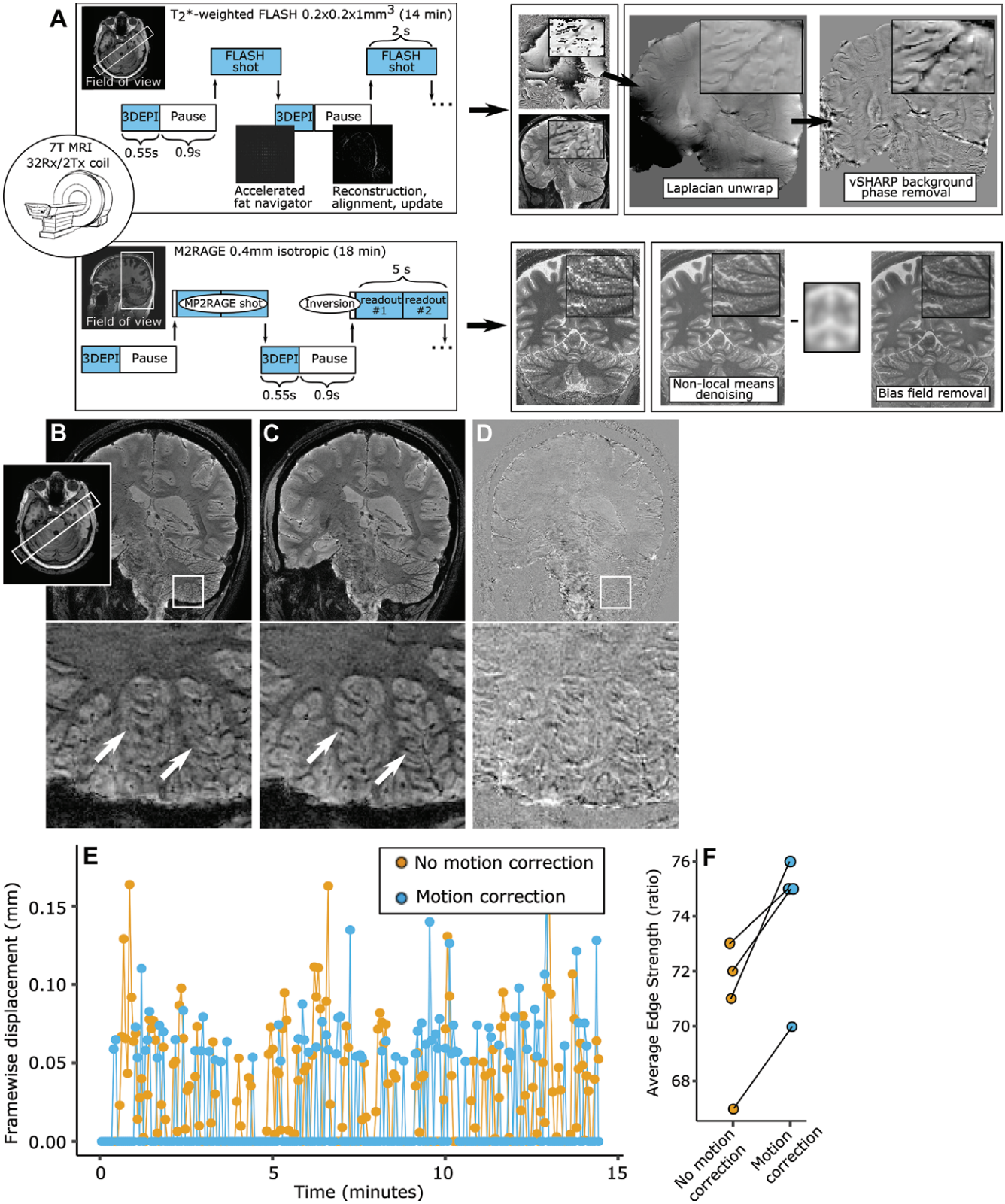

Figure 2: Experimental setup. **(A)** The cerebellar cortical layers were imaged with a T2*-weighted fast low-angle shot (FLASH) sequence and the whole cerebellum with a magnetization-prepared 2 rapid gradient-echo (MP2RAGE) sequence (fields of view, white boxes in **B** and **D**) at 7.0 T. The FLASH and MP2RAGE sequences were segmented and interleaved with lower-resolution whole-head fat navigator three-dimensional echo planar imaging (3DEPI), from which the motion was estimated and corrected prospectively. The phase FLASH images were unwrapped and the background phase removed, revealing contrast in the cerebellar folia. The T1 map was denoised and the bias field removed. vSHARP = varying spherical-kernel sophisticated harmonic artifact reduction for phase data. **(B–D)** Example FLASH images with motion correction off **(B)** and on **(C)** in one individual. Motion correction improved the visibility of individual folia (arrows). The difference between the two acquisitions contained mostly high-intensity small edges (seen in **D**). **(E)** Line graph shows that framewise displacement was similar between acquisitions (F test = 1.01; P = .97). **(F)** Line graph demonstrates that all individuals showed higher average edge strength, indicating reduced blurring when motion correction was used.

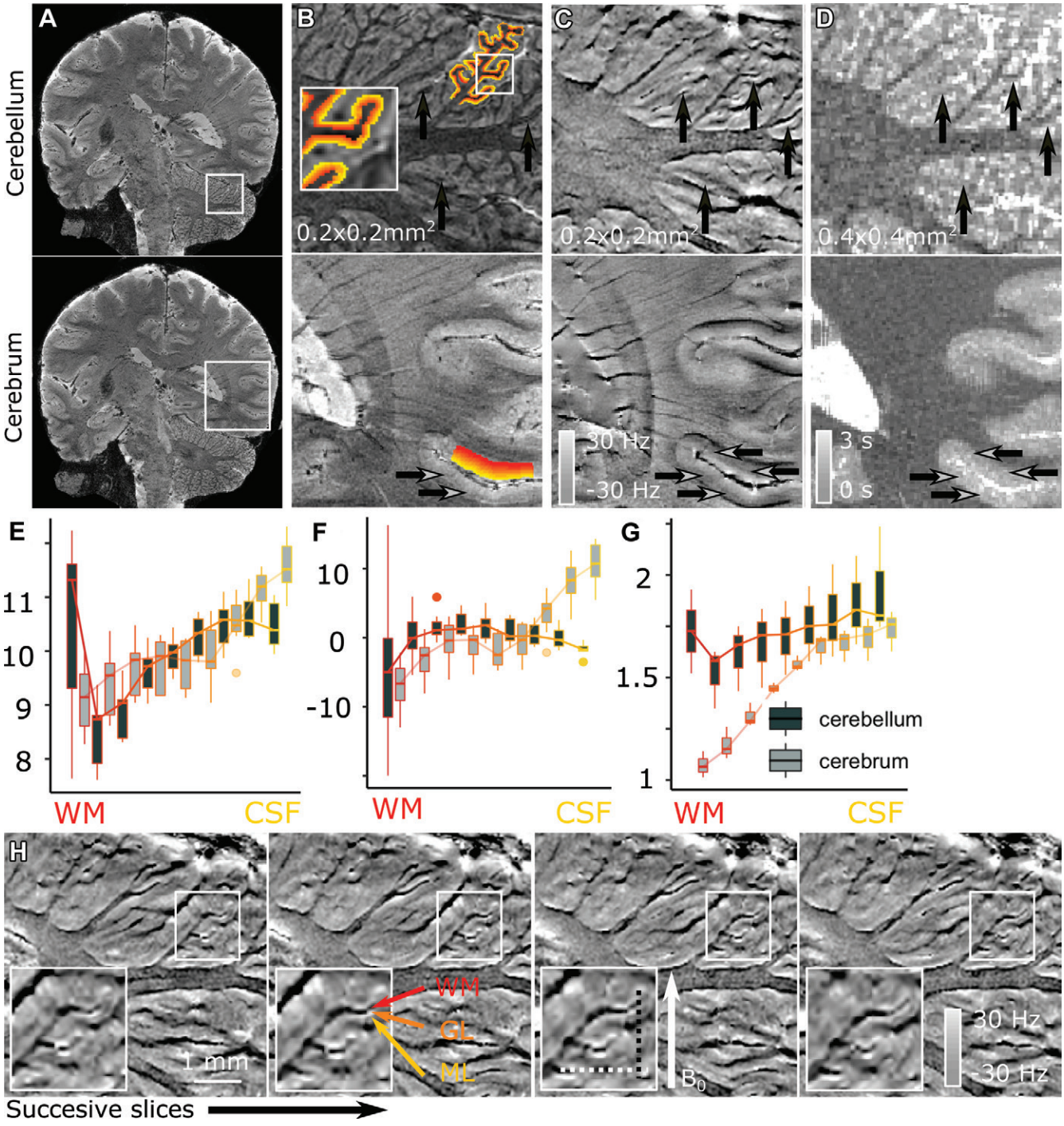

Figure 3: **(A)** Example fast low-angle shot sections of cerebellar (top) and cerebrocortical (bottom) intracortical contrast. Boxes indicate zoomed portions. **(B)** T2*-weighted magnitude image in the cerebellum and cerebrum. The cortical depth was sampled from white matter (WM) (red) to the cerebrospinal fluid (yellow). **(C)** Phase image. Contrast in the cerebellar cortex can be seen (arrows). **(D)** T1 map. **(E–G)** Box and whisker plots show group cortical depth signal profiles for cerebellar (dark gray) and cerebral (light gray) cortex for the T2*-weighted magnitude images **(E)**, phase images **(F)**, and T1 maps **(G)**. Boxes indicate the IQR, midlines show the median, and whiskers represent the minimum and maximum values. CSF = cerebrospinal fluid. **(H)** Successive sections of the extracted phase image of the cerebellar cortex. The intracortical contrast was highly consistent across successive sections. An identification of the granular (GL) and molecular (ML) layers was made. The intracortical contrast was more pronounced perpendicular (white dashed line) rather than parallel (black dashed line) to the B_0 orientation, suggesting a susceptibility origin.

and 2 (respectively), 7°/5°; matrix, 524 × 300 × 150; voxel size, 0.4 × 0.4 × 0.4 mm^3; sensitivity encoding$_{y/z}$, 1.5/1; acquisition time of the MP2RAGE sequence, 14.5 minutes; repetition time of the MP2RAGE shot, 5 seconds; total acquisition time, approximately 18.5 minutes). This two-readout inversion-recovery technique inherently reduces the 7.0-T B_1 inhomogeneities (particularly challenging in the cerebellum [12]) while retaining GM/white matter (WM) contrast (Fig S2, Appendix S2). The same fat navigator was used as for the FLASH sequence. The FOV covered the whole cerebellum (Fig 2A).

Demographic Characteristics of the Study Participants

Age Group and Parameter	Participants Undergoing Imaging with the FLASH Sequence	Participants Undergoing Imaging with the MP2RAGE Sequence
Younger group		
Median age	36 (25–38)	36 (34–38)
F	36 (36–39)	38 (36–40)
M	24.5 (24–25)	33 (29–35)
Sex*		
F	5	4
M	2	3
Older group		
Age of participant 1	57	57
Age of participant 2	62	62

Note.—Data are ages in years unless otherwise indicated. Data in parentheses are IQRs. Both participants in the older group were male. FLASH = fast low-angle shot, MP2RAGE = magnetization-prepared 2 rapid gradient echo.

* Data are numbers of participants.

A lower-resolution magnetization-prepared rapid gradient-echo sequence was used for positioning (FOV, 200 × 220 × 180 mm^3; repetition time msec/echo time msec /inversion time msec, 150/3/1300; flip angle, 7°; matrix, 220 × 244 × 200; voxel size, 0.9 × 0.9 × 0.9 mm^3; sensitivity $encoding_{y/z}$, 2.5/2; acquisition time, 2 minutes). The B_0 field was homogenized within the brain with a second-order shim (MRCodeTool version 1.5.7, Tesla Dynamic Coils).

Image Analysis

For the FLASH image, the tissue phase was derived following Laplacian unwrapping and background-field elimination with use of vSHARP, or the varying spherical-kernel sophisticated harmonic artifact reduction for phase data method (13) (Fig 2A). Six degrees-of-freedom transforms were calculated between the FLASH and MP2RAGE sequences with use of the Advanced Normalization Tools software, version 2.1 (Penn Image Computing and Science Laboratory) (14).

In the magnitude FLASH image, a sample cortical branch was manually selected through three successive sections (Fig 3A–3D), and voxel classification to WM, GM, and cerebrospinal fluid was performed using a signal intensity gradient magnitude plot (Segmentator [15]). The FLASH data were upsampled to 0.1 × 0.1 mm^2 in plane, and the initial voxel classifications were entered into the cortical reconstruction using implicit surface evolution, or CRUISE, algorithm (Nighres version 1.3 [16,17]) to extract non–self-intersecting WM and GM segmentations. Within these segmentations, the magnitude and phase FLASH intensity values and the T1 values from the MP2RAGE sequence were extracted at nine cortical depths, as defined with an equidistant criterion (17). For comparison purposes, an area of interest was drawn in the occipital cortex where prominent intracortical striations exist (Fig 3A–3D).

The T1-weighted images derived from the MP2RAGE sequence were corrected for residual intensity bias (N4 algorithm) and denoised using a spatially adaptive filter (Advanced Normalization Tools software [18]) (Fig 2A). Downsampled versions of the initial 0.4 × 0.4 × 0.4-mm^3 images were created at 0.75 × 0.75 × 0.75 mm^3 and 1 × 1 × 1 mm^3. A signal intensity gradient magnitude was used to extract an initial probability distribution for WM, GM, and cerebrospinal fluid, and non–self-intersecting segmentations were derived as described earlier. The mid GM was estimated with an equidistant criterion, and the output was densely tessellated with a fast-marching algorithm to a mesh (approximately 4.6 million vertices; approximately 25 times the typical FreeSurfer neocortex reconstruction). The resulting surface was computationally unfolded (17,19).

Statistical Analysis

For the MRI sequences acquired with and without prospective motion correction, the frame-to-frame motion distribution variances were compared with an *F* test. The average edge strength ratio (an image sharpness measure) was calculated (20) following brain masking with the FSL Brain Extraction Tool (FMRIB Analysis Group). A paired *t* test was performed to evaluate if improved sharpness was achieved (empirical evidence suggested that the data were similar to a normal distribution). For the healthy young participants, a repeated-measures analysis of variance was performed to examine if the T2* magnitude, T2* phase, and T1 values were differentially dependent on the cerebellar cortical depth. Similarly, for the healthy young participants, a repeated-measures analysis of variance was used to examine if downsampling the initial data affected the derived cortical measures (surface area, thickness, and WM and GM volume). Significant main effects were investigated pairwise with paired *t* tests after Bonferroni adjustment. All tests were performed by N.P. using the R Project software (version 3.5.1, The R Foundation). Statistically significant difference was established at $P < .05$.

Results

Participant Characteristics

The cohort of young participants who underwent imaging with the FLASH sequence consisted of seven participants, with a median age of 36 years (IQR, 25–38 years) (five women and two men) (Table). Our cohort of young participants who underwent imaging with the MP2RAGE sequence consisted of seven participants, with a median age of 36 years (IQR, 34–38 years) (four women and three men). In addition, two healthy older men (aged 57 and 62 years) were recruited and completed both the MP2RAGE and FLASH sequences. In two male participants who underwent imaging with the MP2RAGE sequence, B_1 inhomogeneities were evident in the cerebellum (one was excluded from analysis).

Image Quality and Motion Correction Efficacy

The prospective motion correction preserved the high-resolution image features (Figs 2B–2F, S3), resulting in improved

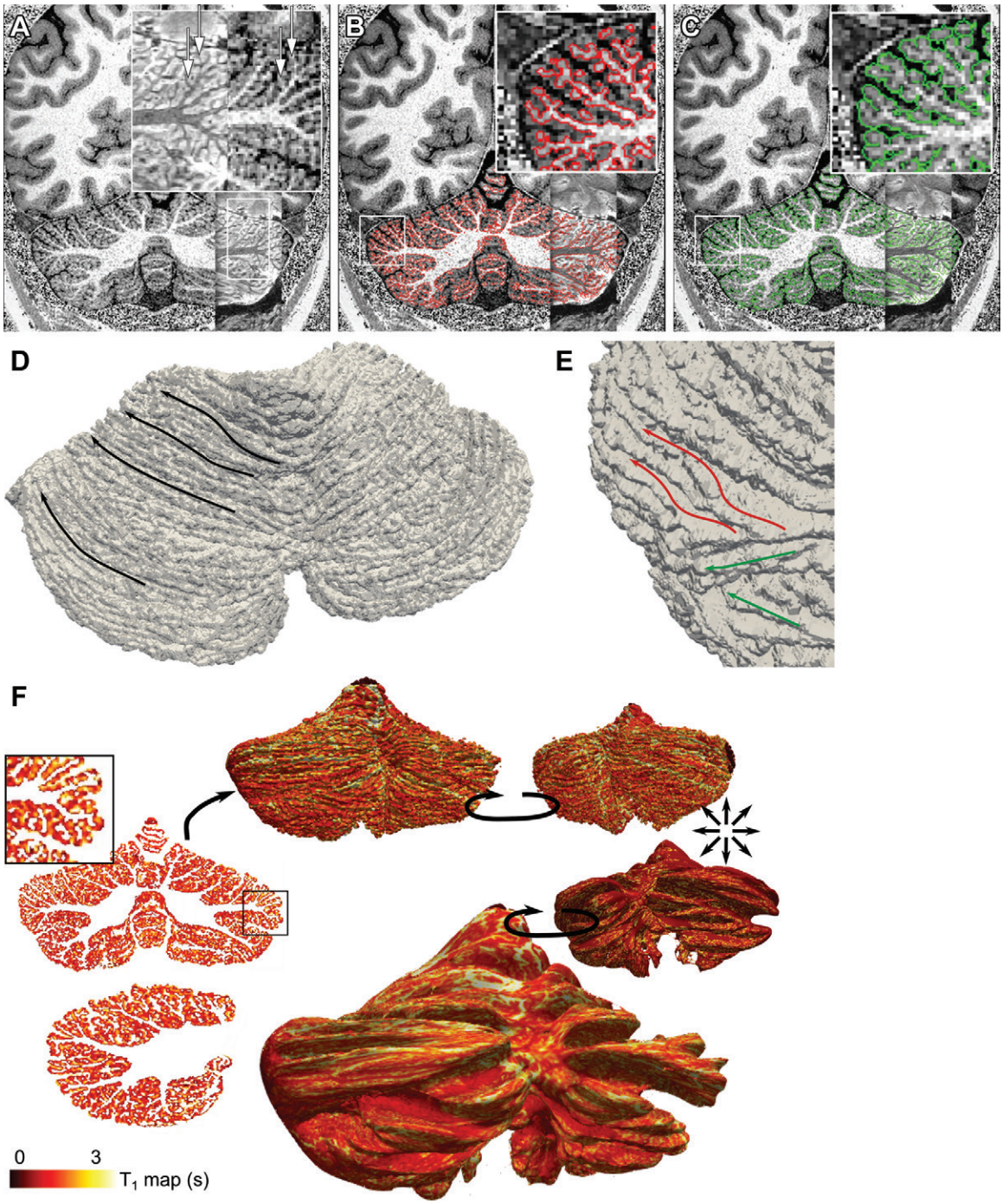

Figure 4: **(A)** Whole–cerebellar cortex T1-weighted image (0.4 mm isotropic). Boxes indicate zoomed portions. The vertical band is the 0.19 × 0.19 × 0.5-mm partial field of view T2*-weighted fast low-angle shot sequence, for reference. At 0.4 mm, individual folia (arrows) can still be resolved. **(B)** White matter segmentations. **(C)** Pial surface segmentations. **(D)** High-fidelity segmentations allow cerebellar surfaces that resolve the characteristic transverse fissures (arrows). **(E)** Splitting folds (wavy arrows) and angulated folds compared with neighboring lobules (straight arrows) can also be resolved. **(F)** Projection of the T1 map cortical ribbon to the surface and surface unfolding (anterior and posterior view). Arrows indicate the projection, rotation, and unfolding processes.

sharpness (higher average edge strength ratio with motion correction [median, 75 {IQR, 73.75–75.25}] than without [median, 71.5 {IQR, 70–72.25}; $t\{3\} = 5.17$; $P = .01$]) despite similar amounts of motion in both acquisitions (F test = 1.01; $P = .97$). Qualitative assessment of both the FLASH and MP2RAGE images indicated visibility of the cerebellar anatomic features, up to individual folia (Figs 3A–3D, S4; Movie 1).

Cerebellar Cortical Layers

In all participants, we visually observed a negative frequency shift in the WM and a positive shift in the deep GM (up to

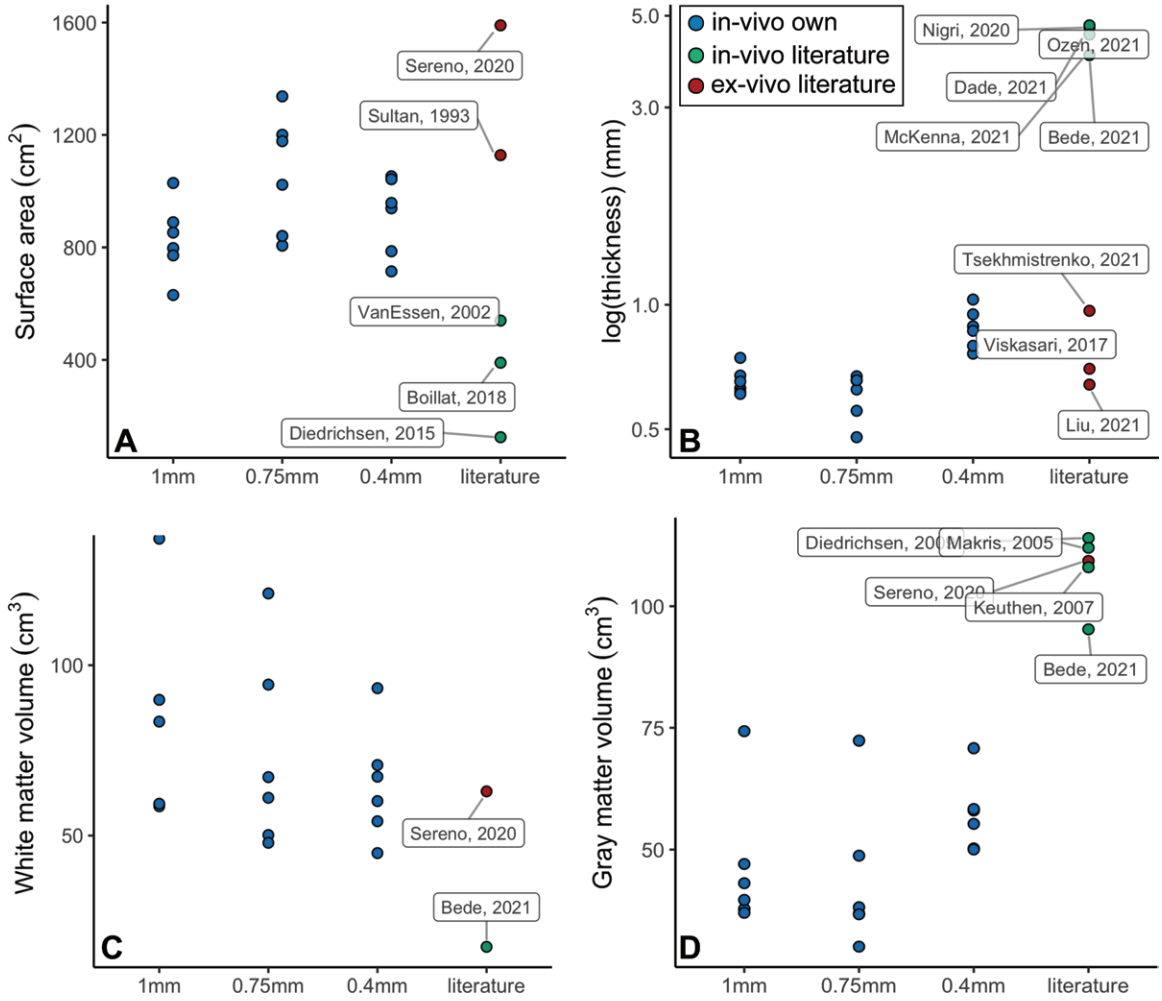

Figure 5: Individual-value plots show estimates compared with reference values (see Table S7 for extended data). Blue dots indicate our in vivo results; red dots, ex vivo literature results; green dots, in vivo literature results. **(A)** Cerebellar cortical surface area estimates. **(B)** Cerebellar cortical thickness estimates. **(C)** White matter volume estimates. **(D)** Gray matter volume estimates.

20–25 Hz when optimally oriented toward B_0) compared with the outer GM in the phase images (Fig 3C). The deep-GM frequency shift colocalized with the expected location of the iron-rich granular layer, as confirmed by the significantly lower signal in the T2*-weighted magnitude (depths: two to four) compared with the outer, sparser-structured molecular layer (depths: five to nine [Fig 3E–3G]; see Tables S1–S3 for statistical parameters). This frequency shift extended across sections, followed the cerebellar foliation, and was confirmed to be related to susceptibility due to its dependence on B_0 orientation (Figs 3H, S5). The myelin-rich striation of the neocortical occipital lobe visually showed a small negative frequency shift and a T1 reduction (Fig 3C, 3D). In sum, signal variations consistent with the granular and molecular layers of the cerebellar cortex were visualized across all individuals.

Cerebellar Segmentations

We next extended our approach to image and segment the entire cerebellar cortex. Our high-spatial-resolution MP2RAGE sequence (0.4 mm isotropic; voxel volume, 0.064 mm^3) allowed discerning individual folia, though with cortical detail loss compared with the partial-coverage FLASH image (Fig 4A). Our signal intensity GM/WM segmentations showed individual folia detail (Figs 4B, 4C, S6).

Cerebellar Cortical Surface

The resulting surface showed the characteristic transverse fissures of the cerebellar cortex, as well as other anatomic details, including splitting folds and lobular folds angulated toward the predominant direction (Fig 4D, 4E). The high-fidelity cerebellar surface allowed us to unfold the transverse fissures of the cerebellar cortex to reveal the continuous cortical sheet (Fig 4F, Movie 2). As an example application, we projected T1 estimates (a myelin-sensitive measure) on the inflated surface (Fig 4F).

Downsampling the data to current state-of-the-art MRI acquisitions reduced the visibility of the cerebellar anatomic features, such as folia (Fig S6), and significantly lowered the estimated cortical thickness (Tables S4–S6). The median cerebellar cortical surface area was estimated at 949 cm^2 (IQR, 825–1021 cm^2), 84% (21) and 60% (1) of the only two previous high-fidelity surface area estimates (both ex vivo and requiring several hours of MRI

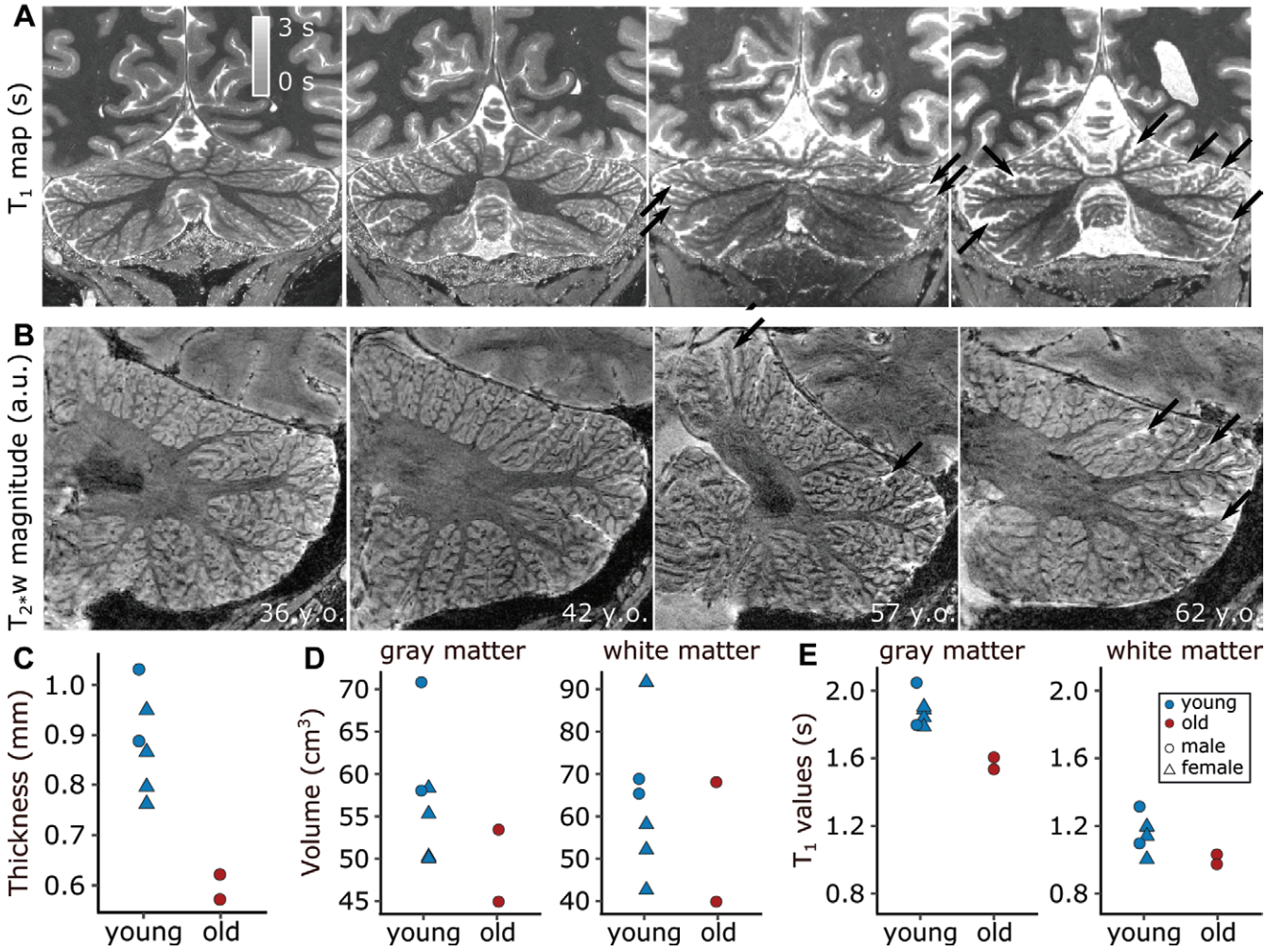

Figure 6: **(A, B)** Example cerebellar sections (increasing in participant age from left to right) from the T1 map **(A)** and T2*-weighted (T_2-w) magnitude image **(B)**. For the older individuals, cerebellar cortical thinning can be seen visually as increased cerebrospinal fluid space (arrows). a.u. = arbitrary units, y.o. = years old. **(C–E)** Individual-value plots show cerebellar measures across cohorts for cortical thickness **(C)**, cerebellar gray and white matter volume **(D)**, and T1 values **(E)**.

scanning to obtain) but 176%–759% larger than previous imaging-based in vivo estimates (Fig 5, Table S7). The median cerebellar cortical thickness was estimated at 0.88 mm (IQR, 0.81–0.93 mm) in agreement with ex vivo reports (0.7–0.8 mm) (22) and four to five times smaller than the current typical imaging-based in vivo estimates. Our median WM volume estimate (64 cm^3 [IQR, 62–69 cm^3]) agreed with the reference ex vivo study (63 cm^3 [1]).

Older Participants

The older participants showed visible cortical thinning in the cerebellum at visual inspection (Fig 6A, 6B). The cerebellar cortical thickness and GM T1 values of both older participants were more than 1.5 times the IQR below the first quartile of the young cohort distribution, suggesting a deviation of these data points from the younger cohort (Fig 6C–6E, Table S8).

Discussion

To date, methods to image the human cerebellum in vivo with fidelity to the level of individual foliations remain lacking. This hinders examining the role of the cerebellum in various disease processes. In this study, we demonstrated that motion-resistant 7.0-T MRI can be used to image the cerebellar cortical layers and to reconstruct and unfold the cerebellar cortical surface while resolving individual foliations. This allows for calculation of quantitative measures, such as the cerebellar cortical surface area and thickness, and examination of correlates of the cerebellar myeloarchitecture, such as T1 values, on the continuous cerebellar cortical sheet.

To achieve between-layer contrast in the cerebellar cortex, we used the higher magnetic susceptibility difference of the deep, iron-rich granular layer and the less neuronally dense superficial molecular layer (9) at 7.0 T. This resulted in consistent visualization of an inner and outer layer–like structure in the cerebellar cortex across participants, likely relating to the granular and molecular layers and in agreement with a previous pilot study, confirmed with histologic examination (9). Spatial resolution limits prohibit the visualization of the middle Purkinje layer. The cerebellar layers are differentially affected in diseases like multiple sclerosis (where extensive demyelination of the molecular layer is observed [2]) or spinocerebellar ataxia type 6, where the Purkinje and molecular layers atrophy while the granular layer is spared (23). The visualization of the cerebellar cortical layers may therefore provide disease markers for prognosis or intervention.

The derivation of clinical cortical measures, such as cortical volume or thickness, relies on accurate GM/WM segmentations to the level of individual folia. In current clinical cerebellar research, the GM/WM segmentations pragmatically rely on anatomic templates to reduce the sensitivity to inadequate spatial or contrast resolution (1). This implicitly smooths over the sublobular anatomy, including the functionally important mediolateral folds. Measures that are commonly used in cerebral clinical research, such as volume or cortical thickness, become unreliable when applied in the cerebellum with typical spatial resolution (≥0.8 mm) (1). Herein, we extracted WM/GM segmentations that distinguished several, though not all, individual folia. There are few ex vivo reference studies (Table S7), but our measures (cortical surface area, cortical thickness, and WM volume) were closer to these ex vivo references compared with previous in vivo studies.

This further allowed us to unfold the cerebellar cortical surface. Cerebellar foliation–level unfolding has not been attempted before in vivo, although it was recently demonstrated ex vivo (and after laborious effort [1]). Despite the highly regular, cylindrical nature of the cerebellar foliation, the curvature of the cerebellar lobules produces a surface with higher intrinsic curvature than that of the cerebrocortical surface (1). We limited the inflation to the lobular level to avoid incurring large distortions (1) but unfolded the mediolateral folds and revealed the deeper folia. The unfolded view may facilitate examining continuous myelination or functional activation differences in clinical conditions, similar to the cerebral cortex (24).

Our study has limitations. First, our study relied on the high signal-to-noise ratio and contrast-to-noise ratio of 7.0-T MRI. Such a field strength is currently rare, although it is becoming increasingly available to clinical researchers. Second, our sample size, while typical for MRI technical development studies (25), was limited, and the method was evaluated in healthy individuals. Third, our 0.19 × 0.19 × 0.5-mm^3 layer visualization sequence did not include the whole cerebellar cortex to limit scan time. Fourth, there is a current dearth of ex vivo reference studies from which to derive reference data. Finally, cerebellum 7.0-T MRI frequently suffers from B_1 inhomogeneities, which were particularly evident in two participants in our study. Image quality can be further enhanced in future implementations using plug-and-play parallel transmit approaches (12).

In summary, 7.0-T MRI with a nonisotropic in-plane resolution of up to 0.19 mm with motion correction provided in vivo visualization of the cerebellar cortical layers and cerebellar surface.

Author contributions: Guarantors of integrity of entire study, **N.P., S.O.D., W.v.d.Z.**; study concepts/study design or data acquisition or data analysis/interpretation, all authors; manuscript drafting or manuscript revision for important intellectual content, all authors; approval of final version of submitted manuscript, all authors; agrees to ensure any questions related to the work are appropriately resolved, all authors; literature research, **N.P., W.v.d.Z.**; clinical studies, **N.P.**; experimental studies, **N.P., M.A., V.O.B., W.v.d.Z.**; statistical analysis, **N.P.**; and manuscript editing, all authors

Data sharing statement: Data generated or analyzed during the study are available from the corresponding author by request.

Disclosures of conflicts of interest: **N.P.** No relevant relationships. **M.A.** No relevant relationships. **S.O.D.** No relevant relationships. **V.O.B.** No relevant relationships. **W.v.d.Z.** Software support from Philips; grant to institution from the Royal Netherlands Academy of Arts and Sciences (KNAW); reduced or waived conference registration fees from the International Society for Magnetic Resonance in Medicine; unpaid positions as the secretary and later chair of the Brain Function Study Group of International Society for Magnetic Resonance in Medicine and on the program committee for the Spinoza Centre for Neuroimaging.

References

1. Sereno MI, Diedrichsen J, Tachrount M, Testa-Silva G, d'Arceuil H, De Zeeuw C. The human cerebellum has almost 80% of the surface area of the neocortex. Proc Natl Acad Sci U S A 2020;117(32):19538–19543.
2. Kutzelnigg A, Faber-Rod JC, Bauer J, et al. Widespread demyelination in the cerebellar cortex in multiple sclerosis. Brain Pathol 2007;17(1):38–44.
3. Wilkins A. Cerebellar dysfunction in multiple sclerosis. Front Neurol 2017;8:312.
4. Klaes A, Reckziegel E, Franca MC Jr, et al. MR imaging in spinocerebellar ataxias: a systematic review. AJNR Am J Neuroradiol 2016;37(8):1405–1412.
5. Luo J. Effects of ethanol on the cerebellum: advances and prospects. Cerebellum 2015;14(4):383–385.
6. Fahle M, Braitenberg V. Some Quantitative Aspects of Cerebellar Anatomy as a Guide to Speculation on Cerebellar Functions. In: Bloedel JR, Dichgans J, Precht W, eds. Cerebellar Functions. Springer, 1985; 186–200.
7. Afacan O, Erem B, Roby DP, et al. Evaluation of motion and its effect on brain magnetic resonance image quality in children. Pediatr Radiol 2016;46(12):1728–1735.
8. Andersen M, Björkman-Burtscher IM, Marsman A, Petersen ET, Boer VO. Improvement in diagnostic quality of structural and angiographic MRI of the brain using motion correction with interleaved, volumetric navigators. PLoS One 2019;14(5):e0217145.
9. Marques JP, van der Zwaag W, Granziera C, Krueger G, Gruetter R. Cerebellar cortical layers: in vivo visualization with structural high-field-strength MR imaging. Radiology 2010;254(3):942–948.
10. de Bruin PW, Koken P, Versluis MJ, et al. Time-efficient interleaved human (23)Na and (1)H data acquisition at 7 T. NMR Biomed 2015;28(10):1228–1235.
11. Bazin PL, Nijsse HE, van der Zwaag W, et al. Sharpness in motion corrected quantitative imaging at 7T. Neuroimage 2020;222:117227.
12. Priovoulos N, Roos T, Ipek Ö, et al. A local multi-transmit coil combined with a high-density receive array for cerebellar fMRI at 7 T. NMR Biomed 2021;34(11):e4586.
13. Li W, Wu B, Liu C. Quantitative susceptibility mapping of human brain reflects spatial variation in tissue composition. Neuroimage 2011;55(4):1645–1656.
14. Avants BB, Tustison NJ, Song G, Cook PA, Klein A, Gee JC. A reproducible evaluation of ANTs similarity metric performance in brain image registration. Neuroimage 2011;54(3):2033–2044.
15. Gulban OF, Schneider M, Marquardt I, Haast RAM, De Martino F. A scalable method to improve gray matter segmentation at ultra high field MRI. PLoS One 2018;13(6):e0198335.
16. Han X, Pham DL, Tosun D, Rettmann ME, Xu C, Prince JL. CRUISE: cortical reconstruction using implicit surface evolution. Neuroimage 2004;23(3):997–1012.
17. Huntenburg JM, Steele CJ, Bazin PL. Nighres: processing tools for high-resolution neuroimaging. Gigascience 2018;7(7):giy082.
18. Tustison NJ, Avants BB, Cook PA, et al. N4ITK: improved N3 bias correction. IEEE Trans Med Imaging 2010;29(6):1310–1320.
19. Tosun D, Rettmann ME, Naiman DQ, Resnick SM, Kraut MA, Prince JL. Cortical reconstruction using implicit surface evolution: accuracy and precision analysis. Neuroimage 2006;29(3):838–852.
20. Zacà D, Hasson U, Minati L, Jovicich J. Method for retrospective estimation of natural head movement during structural MRI. J Magn Reson Imaging 2018;48(4):927–937.
21. Sultan F, Braitenberg V. Shapes and sizes of different mammalian cerebella. A study in quantitative comparative neuroanatomy. J Hirnforsch 1993;34(1):79–92.
22. Liu CJ, Ammon W, Siless V, et al. Quantification of volumetric morphometry and optical property in the cortex of human cerebellum at micrometer resolution. Neuroimage 2021;244:118627.
23. Ishikawa K, Watanabe M, Yoshizawa K, et al. Clinical, neuropathological, and molecular study in two families with spinocerebellar ataxia type 6 (SCA6). J Neurol Neurosurg Psychiatry 1999;67(1):86–89.
24. Fischl B. FreeSurfer. Neuroimage 2012;62(2):774–781.
25. Hanspach J, Nagel AM, Hensel B, Uder M, Koros L, Laun FB. Sample size estimation: current practice and considerations for original investigations in MRI technical development studies. Magn Reson Med 2021;85(4):2109–2116.